Effect of Fe-rich particles and solutes on the creep behavior of 8xxx alloys

Lei Pan, Foisal Ahmed Mirza, Kun Liu, X.-Grant Chen *

Department of Applied Science, University of Québec at Chicoutimi

Saguenay (QC), Canada, G7H 2B1

Keywords: 8xxx Al conductor alloys; Creep properties; Fe-rich intermetallics; Fe solutes; Threshold stress.

* Corresponding author:

X.-Grant Chen,   Tel.: 1-418-545 5011 ext. 2603; Fax: 1-418-545 5012;

E-mail: xgrant_chen@uqac.ca

Effect of Fe-rich particles and solutes on the creep behavior of 8xxx alloys

Abstract

The creep behavior of 8xxx aluminum conductor alloys with different amounts of Fe-rich particles and solutes was investigated. Creep resistance is significantly improved by large amounts of Fe-rich particles and solutes. At 100 °C, a high Fe content of solutes (0.023 wt.%) had a stronger effect on creep resistance than $FeAl_3$ particles, while as the temperature increased to 150 and 200 °C, the effect of a high amount of $FeAl_3$ particles (2.5 vol.%) was stronger than that of Fe solutes. The threshold stress increased with increasing $FeAl_3$ particle and Fe solute contents but decreased with increasing temperature. The increase of the threshold stress due to $FeAl_3$ particles and Fe solutes is independent. The true stress exponent was calculated to be 3.1, 3.8, and 4.5 at 100, 150 and 200 °C, respectively.

1. Introduction

With the rapid growth in the demand for wires and cables, the consumption of electric conductor materials has been significantly increased in the last decade [1-3]. Aluminum conductors have significant advantages in the electrical industry where weight and cost are major factors [4]. The mass resistivity of an aluminum conductor is one-half of that of a copper conductor, meaning that only one-half of the weight of aluminum is required to obtain an equivalent capacity to that of copper [5], making in aluminum conductors an attractive alternative to copper conductors in electrical applications. Particularly, 8xxx aluminum conductor alloys are the most commercialized alloys, such as AA8030 alloys, used in electrical distribution applications within buildings due to their sufficient thermal stability to resist the creep deformation [6,7].

Fe is one of the main alloying elements in 8xxx aluminum conductor alloys and is

traditionally used to enhance the strength of these alloys [5,8]. The strengthening effect arises from the presence of small insoluble Fe-rich dispersion particles that form during solidification and fabrication process [5,9]. The presence of these particles promotes the retardation of the dislocation glide and climb [6,10] and stabilizes the substructure [11]. Zhang et al. [6] reported that the addition of 0.7 wt.% Fe greatly improved the creep resistance of Al−Fe−Cu alloy due to the presence of AlFe dispersoids. In our previous work [12], it was confirmed that the addition of 0.3-0.7 wt.% Fe greatly improved the mechanical properties and creep resistance of 8xxx conductor alloys. Additionally, several investigations have shown that the presence of Fe in solid solution also has a considerable effect on the creep properties of aluminum alloys [13-17]. Sherby et al. [13] proposed that the diffusion of the solute atoms within the subgrain boundaries determined the rate-controlling creep process and observed a decreasing creep rate of pure aluminum after the trace addition of 0.054 wt.% Fe. The effect of Fe on the mechanical properties in other alloy systems (Al-9Si alloys) has also been investigated [18].

In general, in alloys containing particles and solutes, a threshold stress σ_{th} may exist, defined as the lowest stress limit below which creep is not experimentally measurable [10,19,20]. The presence of a threshold stress contributes to the creep strength and affects the stress exponent, with a higher threshold stress leading to a better creep resistance [16,21,22]. Chaudhury et al. [16] observed that the addition of 0.032 wt.% Fe solute atoms to Zn−Al alloys induced the threshold stress and resulted in a considerable increase in the creep resistance. Furthermore, Karnesky et al. [10] reported that in Al-Sc alloys containing two particle populations, the strengthening effect was equivalent to the sum of the individual contributions. We note that little attention has been paid to the combined effects of Fe-rich particles and Fe solutes on the creep deformation of aluminum alloys. Hence, an understanding of the effects of Fe-rich particles and Fe solutes on

the creep behavior of 8xxx aluminum conductor alloys is critical for designing aluminum conductor materials.

Generally, the temperature ranges for creep can be subdivided into three categories: (1) high temperature creep (T > 0.6 T_m), (2) intermediate temperature creep (0.3 T_m < T < 0.6 T_m), and (3) low temperature creep (T < 0.3 T_m) where T_m is the absolute melting point of the alloy [23]. The need for an adequate creep resistance at modest temperatures in light alloys was recognized and explored in several studies [24]. However, most of the works on creep were conducted at high temperatures T > 0.5 T_m [11,13,25]. Sherby et $al.$ [13] studied the effect of Fe on the creep in aluminum at a temperature higher than 200 °C (T > 0.5 T_m) and Marquis et $al.$ [11] studied the presence of the threshold stress of Al-Sc alloys at 300 °C. Very few studies have paid attention to the intermediate temperature creep because the materials generally neither fail nor experience significant plasticity at relatively lower temperatures [23]. To the best of our knowledge to date, no systematic investigation has focused on studying the effect of Fe on the creep behavior of aluminum alloys at the intermediate temperature range (0.4 ~ 0.5 T_m), which seriously limits the further application of 8xxx aluminum conductor alloys [26]. Thus, the aim of the present work was to investigate the influences of both Fe-rich particles and Fe solutes on the creep behavior of 8xxx aluminum conductor alloys in a 100-200 °C temperature range. Additionally, the creep mechanism was discussed based on the values of the true stress exponent.

2. Materials and experimental procedure

The materials used in this study were an 8xxx aluminum alloy with 0.3% Fe (A3) and 0.7% Fe (A7) (all of the alloy compositions in this work are in wt.% unless otherwise indicated). The chemical compositions of the experimental alloys are given in Table 1. The present alloys were produced and fabricated into 9.5 mm supply rods for drawn wire by hot extrusion from DC cast

billets. The details of the fabrication process are described elsewhere [2]. Experimental alloys with two Fe contents were designed to have different amounts of Fe-rich particles to quantify the effect of Fe-rich particles on the creep properties. Furthermore, to obtain a large difference of the Fe solute levels, the alloys were subjected to two thermal holding treatments, the first at 640 °C for 24 h (high thermal, HT) and another consisting of two step treatments (low thermal, LT): 640 °C for 24 h (aimed to obtain the similar grain structure and same type of Fe-rich particles as HT treatment) + 500 °C for 24 h (aimed to obtain a low Fe solute content in aluminum due to the temperature dependent solubility [13,27]). These conditions were designated as A3H and A3L for A3 alloys after HT and LT treatments and A7H and A7L for A7 alloys after HT and LT treatments, respectively. All of the thermal holding treatments were followed by a direct water quench to keep the Fe solutes in the aluminum matrix.

To quantitatively analyze the Fe-rich particle distribution, the alloys treated by thermal holding were examined by scanning electron microscopy (SEM). All samples were sectioned parallel to the extrusion direction along the centerline and then polished. X-ray energy-dispersive spectroscopy (EDS) attached to a transmission electron microscopy (TEM) was used to analyze the chemical composition of the dispersoids. In addition, an image analysis technique was used to measure the size and volume fraction of the Fe-rich particles. Furthermore, the electrical conductivity was measured at room temperature on the cylindrical samples (9.5 mm in diameter and 200 mm in length) after different thermal holding treatments using a Megger DLRO10HD resistance ohmmeter to detect the solute content.

Compressive creep tests were performed on the samples (9.5 mm in diameter and 19 mm in length) at temperatures from 100 to 200 °C and under various applied loads ranging from 20 to 60 MPa. The samples were subjected to stepwise loading, where the load changed to a new value

after the second creep stage had been established for a given load. To ensure thermal stability, all specimens were held at the test temperature for 1 h prior to loading.

3. Results

3.1 Distribution of Fe-rich intermetallics and Fe solutes

Fig. 1 shows the SEM back-scattered images of A3 and A7 alloys after two thermal holding treatments. As shown in Figs. 1(a)-(d), a large number of Fe-rich intermetallic particles was observed (white particles indicated by arrows) that were uniformly distributed throughout the matrix. The particles were identified as the equilibrium Al$_3$Fe phase from the electron backscattered diffraction (EBSD) results reported by Shakiba *et al.* [28]. The average sizes of the Fe-rich particles were measured to be similar (~0.36 μm) under all four conditions. Furthermore, it is found that the volume fraction of the particles is similar in alloys with the same Fe content either after the "HT" or "LT" heat treatment. For instance, as shown in Figs. 1(c)-(d), the Fe content is 4.26 vol.% in A7H to 4.33 vol.% in A7L, respectively. However, there is a large difference in the volume of the Fe-rich intermetallics in Alloys A3 and A7, which rapidly increased with increasing Fe content. The calculated vol.% from image analysis was approximately 1.8 vol.% in Alloys A3L and A3H while it was as high as approximately 4.3 vol.% in Alloys A7L and A7H.

On the other hand, the Fe solute level after the thermal holding treatment was evaluated by electrical conductivity (EC) measurements. Based on the relationship between the EC and concentration of the alloying elements in the solid solution, a quantitative estimation of the Fe solute content was calculated according to the following equation [29,30]:

$$\frac{1}{EC} = 0.0267 + 0.032Fe_{ss} + 0.002Cu_{ss} + 0.0068Si_{ss} + 0.003Mg_{ss} + 0.0003Particle\% \tag{1}$$

where, Fe_{ss}, Cu_{ss}, Si_{ss}, and Mg_{ss} are the weight percentages of these elements in the solid solution and particle % is the volume fraction of the particles. The calculated Fe solute levels under different conditions are summarized in Table 2. It is clearly seen that after the HT treatment the alloys showed a comparatively higher Fe solute level compared to these alloys after the LT treatment. In addition, the equilibrium solubility of Fe in a binary Al-Fe system (Fig. 2) is also introduced to estimate the solute Fe levels [27]. As shown in Table 2, it is found that the calculated Fe solute contents are in good agreement with the theoretical values from the Al−Fe phase diagram. It can be seen that the Fe solute level is approximately 0.03% after the "HT" treatment (A3H and A7H) while it is 0.005-0.008% after the "LT" treatment (A3L and A7L).

3.2 Creep behavior

Fig. 3 shows typical compressive creep curves of all of the alloys tested at 100 ℃ under a constant load of 45 MPa for 100 h. These curves are representative of the data obtained for all of the experimental conditions. It was found that the total creep strain significantly decreased from 0.096 in the A3L alloy to 0.001 in the A7H alloy (Fig. 3(a)) with the increase of the Fe-rich particle content from 1.8 to 4.3 vol.% and of the Fe solute level from 0.008 to 0.031 wt.%. Two creep stages were observed in the compressive creep tests. In the initial stage, the creep strain greatly increased with increasing time at a decelerating rate due to work hardening (primary creep stage, $d\dot{\varepsilon}/dt$ <0), and then, the primary creep stage transitions to the second stage, where the creep strain increased at a nearly constant rate (quasi-steady stage, $d\dot{\varepsilon}/dt \approx 0$). The minimum creep rate, $\dot{\varepsilon}_m$, was calculated as the average creep rate in the second stage, as shown in Fig. 3(b). It was found that with the increasing content of FeAl₃ particles and Fe solutes, $\dot{\varepsilon}_m$ decreased significantly from 2.3×10^{-7} s^{-1} in the A3L alloy to 2.2×10^{-8} s^{-1} in the A3H alloy (the Fe solutes level increased from 0.008 to 0.031 wt.%), to 3.7×10^{-8} s^{-1} in the A7L alloy (the

FeAl$_3$ particles increased from 1.8 to 4.3 vol.%), and further to 4.9×10^{-10} s^{-1} in the A7H alloy (the amount of both FeAl$_3$ particles and Fe solutes increased). In conclusion, higher amounts of FeAl$_3$ particles and Fe solutes are highly beneficial to the creep resistance, probably due to the pining and impeding effects of both particles and solutes on the dislocation movement [6,16].

To better understand the effects of FeAl$_3$ particles and Fe solutes on the creep behavior, further creep tests were conducted at various temperatures and under different applied stresses. Fig. 4 shows the minimum creep rate $\dot{\varepsilon}_m$ as a function of applied stress σ at 100, 150, and 200 °C. It can be seen that A7H showed the highest creep resistance; followed by A3H and A7L, which displayed moderate creep resistance; and finally, the A3L alloy that showed the lowest creep resistance. At 100 °C, A3H is slightly more creep resistant than A7L, but at 150 and 200 °C, A3H was less creep resistant than A7L. For a given temperature, the stress dependence is apparently given by a straight line, implying a constant apparent stress exponent, n_a, (defined as $\partial ln\dot{\varepsilon}_m/\partial ln\sigma$) [10]. The apparent stress exponent value n_a varies between 7.7 and 13.5 for alloys at the tested temperatures. The value of n_a was much larger than that for pure Al ($n = 3-5$), indicative of the presence of threshold stress analogous to that of the dispersion strengthened alloys [31].

The values of the threshold stress in the studied alloys at various temperatures were estimated by extrapolating the linear fitting, as proposed by Li *et al.* [20]. For example, the extrapolation of the fitted lines to a minimum creep rate of 10^{-10} s^{-1} (Fig. 5(a)) gives a threshold stress σ_{th} of 15.8, 13.5, and 11.5 MPa for the A3L alloys at 100, 150 and 200 °C, respectively. Fig. 5(b) shows the threshold stresses for all of the alloys at different test temperatures. It can be clearly seen that the value of σ_{th} decreased with increasing creep temperature for all of the temperature conditions. At a constant temperature, the A7H (high Fe particle and solute content)

showed the highest σ_{th}, followed by the A3H (high Fe solutes) and A7L (high Fe particles) alloys, which displayed relatively high σ_{th} values, and the smallest σ_{th} was obtained for the A3L alloy (low Fe particle and solute content), showing that the synergistic effects of FeAl$_3$ particles and Fe solutes on the creep properties. At 100 °C, the A3H alloy showed a higher σ_{th} than the A7L alloy (28.9 vs 25.9 MPa), indicating the stronger strengthening effect of the Fe solutes compared to that of the FeAl$_3$ particles. With the temperature increasing to 150 and 200 °C, the A3H alloy displayed a lower σ_{th} compared to the A7L alloy (19.6 vs 22.0 MPa at 150 °C and 15.7 vs 18.1 MPa at 200 °C), demonstrating the stronger strengthening effect of the FeAl$_3$ particles than the Fe solutes.

After determining the threshold stress, the creep behavior of the alloys can be generally described by a modified power law equation [6,10], in which the true stress exponents can be determined:

$$\dot{\varepsilon}_m = A_0 \left(\frac{\sigma - \sigma_{th}}{G}\right)^{n_t} exp\left(-\frac{Q}{RT}\right) \tag{2}$$

where $\dot{\varepsilon}_m$ is the minimum creep rate, σ is the applied stress and σ_{th} is the threshold stress, $\sigma - \sigma_{th}$ is the effective stress, n_t is the true stress exponent, A_0 is a dimensionless constant, G is the shear modulus, Q is the activation energy, R is the universal gas constant and T is the absolute temperature.

Fig. 6 shows the plots of the minimum creep rate $\dot{\varepsilon}_m$ against the effective stress $\sigma - \sigma_{th}$ on a logarithmic scale with the slopes of the plots giving the values of the true stress exponent n_t. In literature, n_t has been frequently used to identify the mechanisms that control the creep process. Based on the different n_t values, the creep mechanisms are theoretically estimated as follows: n_t = 3, for the creep controlled by the viscous glide processes of dislocations [32], n_t = 5, for the creep

9

controlled by the high-temperature dislocation climb [10], and $n_t = 8$ for the lattice diffusion-controlled creep with a constant structure [33]. It was found that the n_t values are between 2.8 and 4.8 for all temperatures, indicating that the dislocation glide and climb controls creep deformation in the experimental alloys. At 100 °C, the n_t values varied from 2.8 to 3.4, indicating that the dislocation glide is the dominated rate-controlling deformation mechanism. As the creep temperature increased to 200 °C, more slip systems are activated and the n_t values are between 4.1 to 4.8, revealing that the dislocation climb is the dominant deformation mechanism. Similar results were reported by Ishikawa et al. [34] and Sherby et al. [13] who postulated that the dislocation glide was responsible for the creep in pure aluminum at 100 °C with a true stress exponent of 3.0 and that the dislocation climb dominated the creep deformation for pure aluminum at 200 °C with a true stress exponent of 4.4, respectively.

4. Discussion

To understand the individual and combined effects of the FeAl$_3$ particles and Fe solutes on the creep properties, the increments of the threshold stress $\Delta\sigma_{th}$ due to the FeAl$_3$ particles $\Delta\sigma_{th}(P)$ and Fe solutes $\Delta\sigma_{th}(S)$ at various temperatures are calculated based on the data presented in Fig. 5(b), as listed in Table 3. The relationship between the total $\Delta\sigma_{th}$, and individual $\Delta\sigma_{th}(P)$ and $\Delta\sigma_{th}(S)$ with increasing temperature is plotted in Fig. 7. In general, the increment in the threshold stress $\Delta\sigma_{th}$ can be expressed by the sum of the $\Delta\sigma_{th}(P)$ for the particles and $\Delta\sigma_{th}(S)$ for the Fe solutes [11]:

$$\Delta\sigma_{th} = \Delta\sigma_{th}(P) + \Delta\sigma_{th}(S) \tag{3}$$

It can be seen that both $\Delta\sigma_{th}(S)$ and $\Delta\sigma_{th}(P)$ decrease with increasing temperature, but the rate of the $\Delta\sigma_{th}(S)$ decrease is higher than that for $\Delta\sigma_{th}(P)$, suggesting a stronger temperature

sensitivity of Fe solutes compared to that of FeAl$_3$ particles. The $\Delta\sigma_{th}$ value from A7H−A3L is very close to the sum of theindividually calculated values of $\Delta\sigma_{th}$(P) (FeAl$_3$ particle contribution from A7L−A3L and A7H−A3H) and $\Delta\sigma_{th}$(S) (Fe solute contribution from A3H−A3L and A7H−A7L), indicating that strengthening occurs due to the combined effects of both FeAl$_3$ particles and Fe solutes, but the contributions of the FeAl$_3$ particles and Fe solutes are independent.

Since the dislocation mechanism controls the creep deformation, this could be explained by the combined effects of FeAl$_3$ particles and Fe solutes in impeding the movement of dislocations [10,35], which means that the stress required to generate the dislocation movement is higher than for a dislocation interaction with either the particles or the solute atoms. Similar results were reported by Karnesky et al. [10] for the creep process at 300 °C in Al alloys with two particle populations (Al$_2$O$_3$ incoherent dispersoids and Al$_3$Sc precipitates) where the overall threshold stress is equivalent to the sum of both contributions of two populations.

4.1 Effect of Fe-rich particles

The effect of the FeAl$_3$ particles on the threshold stress could be due to the interaction between the dislocations and incoherent dispersion particles [35-37]. The most common explanation for σ_{th} is the stress required to cause dislocation bowing between the particles, named Orowan stress σ_{or}, which is given by [36],

$$\sigma_{or} = 0.84M \frac{Gb}{(\lambda - d)} \qquad (4)$$

where M is the Taylor factor, d is the average particle diameter, and λ is the inter-particle spacing. On the other hand, the attractive interaction between the particles and dislocations leads to the dislocation climb over the particles, so that the threshold stress may be associated with the

11

stress (σ_d) required to detach a dislocation from the departure side of an obstacle, as given by [35]:

$$\sigma_d = \sigma_{or}\sqrt{1-K^2} \tag{5}$$

where K is the relaxation parameter that has values between 0 (maximum attractive interaction) and 1 (no attractive interaction). The corresponding average inter-particle spacing λ, can be calculated according to [10]:

$$\lambda = d\left(\sqrt{\frac{\pi}{4f}} - 1\right) \tag{6}$$

where f is the volume fraction of the particles. Therefore, taking $M = 3.06$ and $K = 0.85$ [37], the calculated values of both threshold stresses (σ_{or} and σ_d) are given in Table 4. The increment of the Orowan stress ($\Delta\sigma_{or}$) was calculated as 11.1 MPa for A7L−A3L and A7H−A3H at 100 °C due to the volume fraction increase of the FeAl$_3$ particles; this value is close to that of the experimental estimated $\Delta\sigma_{th}(P)$ value of 10 MPa, as shown in Table 3. The ratio ($\Delta\sigma_{th}/\Delta\sigma_{or}$) was calculated to be 0.91 and 0.92 for A7L−A3L and A7H−A3H, respectively. Therefore, it can be concluded that the Orowan dislocation looping is the dominant factor responsible for the threshold stress. However, the values obtained from the detachment model $\Delta\sigma_d$ (the same values of 5.8 MPa for A7L−A3L and for A7H−A3H, respectively) are much lower than for the experimental determined threshold stress $\Delta\sigma_{th}(P)$.

At the high temperature of 200 °C, the experimental determined $\Delta\sigma_{th}(P)$ was 6.6 and 6.8 MPa for A7L−A3L and A7H−A3H, respectively, which are very close to the detachment stress $\Delta\sigma_d$ (as shown in Table 4). The ratio ($\Delta\sigma_{th}/\Delta\sigma_d$) was calculated to be the same as 1.2, which was ontained for A7L−A3L and A7H−A3H. Therefore, the origin of the threshold stress may be changed from Orowan stress at 100 °C to dislocation detachment stress at 200 °C. This is consistent with the creep mechanism changes from the dislocation glide to the climb as the

temperature is increased from 100 to 200 °C as shown in Fig. 6. Similar results were reported by Kloc *et al*. [37] during creep deformation in the 2024 aluminum alloy where the estimated threshold stress decreased from a value close to that of Orowan stress to a value close to the value of detachment stress with increasing creep temperature.

4.2 Effect of Fe solutes

Although the amount of Fe solutes in both low and high F content alloys appears to be small (0.03% in the HT condition), Fe solutes can have a considerable impact on the creep properties, such as the minimum creep rate (Fig. 3(b)) and threshold stress (Fig. 7). The contribution to the creep properties was greatly increased by the increasing content of Fe solutes, as shown in Figs. 3 and 7, which may be attributed to the Fe-solute-diffusion-controlled creep deformation, as proposed by Sherby *et al.* [13,17,28]. It is suggested that the Fe solutes could segregate at the dislocations at an early stage of creep deformation, reducing the energy of dislocation. During the creep process, the initial stress field from the pile-up dislocation occurs under the applied shear stress and is balanced by the stress field from the subgrain boundary dislocations. Then, the opposing stresses from the subgrain boundaries and pile-up dislocations during creep deformation are cyclically relaxed by the diffusion of the Fe solutes in the subgrain boundaries. Thus, the pile-up dislocation is allowed to glide or climb through the boundaries, and a creep deformation of the material occurs. Due to a rather lower diffusion rate of Fe in aluminum (as shown in Fig. 8), the pile-up dislocations were strongly hindered at the subgrain boundaries by the Fe solute atoms. Sherby *et al*. [13] reported that the addition of 200 ppm Fe in solution could significantly decreased the minimum creep rate by a factor of 10^6 compared to the same aluminum without the Fe solution, which was attributed to the low Fe solute diffusion rate in the subgrain boundary region. The high pinning effect of the Fe solutes results in a high external

stress (threshold stress), which is required to cause the dislocation movement, as confirmed by the high value of the threshold stress (σ_{th}(S)) as shown in Table 3.

Furthermore, the improvement of the threshold stress due to the Fe solutes decreases with increasing temperature, as shown in Fig. 7 and Table 3, which can be attributed to the increasing diffusion rate of Fe. As shown in Fig. 8, the diffusion rate of Fe in Al rapidly increases with temperature. For instance, the Fe diffusion rate is 6.4×10^{-32} m^2/s at 100 °C but it increases sharply to 2.6×10^{-25} m^2/s at 200 °C (Fig. 8). Therefore, the faster diffusion weakens the pinning ability on the dislocation slip and decrease the threshold stress.

5. Conclusions

The creep behavior of 8xxx aluminum conductor alloys containing different amounts of incoherent Fe-rich particles and Fe solutes was studied. The following conclusions can be drawn from this investigation:

1. The presence of FeAl$_3$ particles and Fe solutes in 8xxx alloys significantly improved the creep resistance simultaneously for all test temperatures and stress levels, with the strengthening effect decreasing with increasing temperature.

2. At 100 °C, the addition of Fe solutes (0.023 wt.%) had a stronger effect on the creep resistance than the presence of FeAl$_3$ particles (2.5 vol.%), while at 150 and 200 °C, the high amount of the FeAl$_3$ particles (2.5 vol.%) had a stronger effect than the presence of Fe solutes (0.023 wt.%).

3. The threshold stress was greatly increased with the increasing content of FeAl$_3$ particles and Fe solutes. The strengthening effect due to the FeAl$_3$ particles and Fe solutes was

14

independent and its value is equal to the sum of the individual contribution.

4. The threshold stress decreased with increasing temperature. For the particle contribution, the value was decreased with increasing temperature due to the strengthening mechanism changing from Orowan stress at 100 °C to detachment stress at 200 °C, while the contribution of the Fe solutes strongly decreased with increasing temperature due to the rapid increase of the diffusion rate of Fe in Al at a higher temperature.

5. With the increasing creep temperature from 100 to 150 °C and further to 200 °C, the true stress exponent increases from 3.1 to 3.8 and further to 4.5, respectively.

References

1. V. M. Sizyakov, V. Y. Bazhin, and A. A. Vlasov: 'Status and prospects for growth of the aluminum industry', *Metallurgist*, 2010, **54**, 409-414.

2. L. Pan, B. Bourassa, and X. G. Chen: 'Effect of thermomechanical processing on electrical and mechanical properties of aluminum conductor alloys', *Mater. Sci. Forum*, 2014, **794-796**, 1121-1126.

3. W. H. Yuan and Z. Y. Liang: 'Effect of Zr addition on properties of Al-Mg-Si aluminum alloy used for all aluminum alloy conductor', *Mater. Des.*, 2011, **32**, 4195-4200.

4. W. W. Zhou, B. Cai, W. J. Li, Z. X. Liu, and S. Yang: 'Heat-resistant Al-0.2Sc-0.04Zr electrical conductor', *Mater. Sci. Eng. A*, 2012, **552**, 353-358.

5. H. J. Mcqueen, E. H. Chia, and E. A. Starke: 'Fe-particle-stabilized aluminum conductors',

JOM, 1986, **38**, 19-24.

6. X. Y. Zhang, H. Zhang, X. X. Kong, and D. F. Fu: 'Microstructure and properties of Al-0.70Fe-0.24Cu alloy conductor prepared by horizontal continuous casting and subsequent continuous extrusion forming', *Trans. Nonferrous Met. Soc. China*, 2015, **25**, 1763-1769.

7. C. Olin: 'Aluminum alloy conductor', US Patent 3711339, 1973.

8. M. Jablonski, T. Knych, and B. Smyrak: 'Effect of iron addition to aluminium on the structure and properties of wires used for electrical purposes', *Mater. Sci. Forum*, 2011, **690**, 459-462.

9. H. J. Mcqueen, K. Conrod, and G. Avramovic-cingara: 'The hot-working characteristics of eutectic-rod-stabilized conductor alloys', *Can. Metall. Quart.*, 1993, **32**, 375-386.

10. R. A. Karnesky, L. Meng, and D. C. Dunand: 'Strengthening mechanisms in aluminum containing coherent Al_3Sc precipitates and incoherent Al_2O_3 dispersoids', *Acta Mater.*, 2007, **55**, 1299-1308.

11. E. A. Marquis, D. N. Seidman, and D. C. Dunand: 'Effect of Mg addition on the creep and yield behavior of an Al-Sc alloy', *Acta Mater.*, 2003, **51**, 4751-4760.

12. L. Pan, K. Liu, F. Breton, and X.-G. Chen: 'Effect of Fe on Microstructure and properties of 8xxx aluminum conductor alloys', *J. Mater. Eng. Perform.,* 2016, online published in Oct 2016, DOI: 10.1007/s11665-016-2373-0.

13. O. D. Sherby, A. Goldberg, and O. A. Ruano: 'Solute-diffusion-controlled dislocation creep in pure aluminium containing 0.026 at.% Fe', *Philos. Mag.*, 2004, **84**, 2417-2434.

14. R. I. Babicheva, S. V. Dmitriev, Y. Zhang, S. W. Kok, N. Srikanth, B. Liu, and K. Zhou: 'Effect of grain boundary segregations of Fe, Co, Cu, Ti, Mg and Pb on small plastic deformation of nanocrystalline Al', *Comp. Mater. Sci.*, 2015, **98**, 410-416.

15. A. V. Kazantzis, Z. G. Chen, and J. T. M. De Hosson: 'Deformation mechanism of aluminum-magnesium alloys at elevated temperatures', *J. Mater. Sci.*, 2013, **48**, 7399-7408.

16. P. K. Chaudhury, K. T. Park, and F. A. Mohamed: 'Effect of Fe on the Superplastic Deformation of Zn-22 pct Al', *Metall. Mater. Trans. A*, 1994, **25**, 2391-2401.

17. O. D. Sherby and O. A. Ruano: 'Rate-controlling processes in creep of subgrain containing aluminum materials', *Mater. Sci. Eng. A*, 2005, **410**, 8-11.

18. J. Malavazi, R. Baldan, and A. Augusto Couto: 'Microstructure and mechanical behaviour of Al_9Si alloy with different Fe contents', *Mater. Sci. Technol.,* 2015, **31**, 737-744.

19. P. K. Chaudhury and F. A. Mohamed: 'Effect of impurity content on superplastic flow in the Zn-22% Al alloy', *Acta Metall.*, 1988, **36**, 1099-1110.

20. Y. Li and T. G. Langdon: 'A simple procedure for estimating threshold stresses in the creep of metal matrix composites', *Scripta Mater.*, 1997, **36**, 1457-1460.

21. S. P. Deshmukh, R. S. Mishra, and I. M. Robertson: 'Investigation of creep threshold stresses using in situ TEM straining experiment in an $Al-5Y_2O_3-10SiC$ composite', *Mater. Sci. Eng. A*, 2010, **527**, 2390-2397.

22. F. Naghdi and R. Mahmudi: 'Impression creep behavior of the extruded Mg-4Zn-0.5Ca and

Mg-4Zn-0.5Ca-2RE alloys', *Mater. Sci. Eng. A*, 2014, **616**, 161-170.

23. M. E. Kassner and K. Smith: 'Low temperature creep plasticity', *J. Mater. Res. Technol.*, 2014, **3**, 280-288.

24. G. W. Greenwood: 'Reflections on creep: a review of the MST archive', *Mater. Sci. Technol.,* 2013, 29, 893-899.

25. W. J. Li, B. Cai, Y. C. Wang, Z. X. Liu, and S. Yang: 'Creep of Al-0.2Sc-0.04Zr alloys after different cold-rolling and ageing combinations', *Mater. Sci. Eng. A*, 2014, **615**, 148-152.

26. K. W. Barber and K. J. Callaghan: 'Improved overhead line conductors using aluminum alloy 1120', *IEEE Transactions on Power Delivery.*, 1995, **10**, 403-409.

27. C. M. Allen, K. A. Q. O'Reilly, B. Cantor, and P. V. Evans: 'Intermetallic phase selection in 1XXX Al alloys', *Prog. Mater. Sci.*, 1998, **43**, 89-170.

28. M. Shakiba, N. Parson, and X. G. Chen: 'Effect of homogenization treatment and silicon content on the microstructure and hot workability of dilute Al-Fe-Si alloys', *Mater. Sci. Eng. A*, 2014, **619**, 180-189.

29. Q. L. Zhao, B. Holmedal, and Y. J. Li: 'Influence of dispersoids on microstructure evolution and work hardening of aluminium alloys during tension and cold rolling', *Philos. Mag.*, 2013, **93**, 2995-3011.

30. A. Mamala and W. Sciezor: 'Evaluation of the effect of selected alloying elements on the mechanical and electrical aluminium properties', *Arch. Metall. Mater.*, 2014, **59**, 413-417.

31. S. P. Deshmukh, R. S. Mishra, and K. L. Kendig: 'Creep behavior and threshold stress of an extruded Al-6Mg-2Sc-1Zr alloy', *Mater. Sci. Eng. A*, 2004, **381**, 381-385.

32. A. H. Monazzah, A. Simchi, and S. M. S. Reihani: 'Creep behavior of hot extruded Al-Al_2O_3 nanocomposite powder', *Mater. Sci. Eng. A*, 2010, **527**, 2567-2571.

33. Y. Li and T. G. Langdon: 'An examination of a substructure-invariant model for the creep of metal matrix composites', *Mater. Sci. Eng. A*, 1999, **265**, 276-284.

34. K. Ishikawa, H. Okuda, and Y. Kobayashi: 'Creep behaviors of highly pure aluminum at lower temperatures', *Mater. Sci. Eng. A*, 1997, **234**, 154-156.

35. H. Watanabe, T. Mukai, and K. Higashi: 'Influence of temperature and grain size on threshold stress for superplastic flow in a fine-grained magnesium alloy', *Metall. Mater. Trans. A*, 2008, **39A**, 2351-2362.

36. Y. Li, S. R. Nutt, and F. A. Mohamed: 'An investigation of creep and substructure formation in 2124 Al', *Acta Mater.*, 1997, **45**, 2607-2620.

37. L. Kloc, S. Spigarelli, E. Cerri, E. Evangelista, and T. G. Langdon: 'Creep behavior of an aluminum 2024 alloy produced by powder metallurgy', *Acta Mater.*, 1997, **45**, 529-540.

Tables

Table 1 Chemical compositions of the experimental alloys (wt.%).

Alloys	Fe	Cu	Si	Mg	Al
A3	0.30	0.01	0.025	0.001	Bal.
A7	0.70	0.01	0.023	0.001	Bal.

Table 2 Concentrations of Fe solutes in the samples.

Specimens	EC measured, MS/m	Fe solutes estimated by EC values, wt.%	Fe solutes calculated from Al−Fe phase diagram, wt.% [24]
A3L	36.1	0.008	0.007
A3H	35.2	0.031	0.040
A7L	35.3	0.005	0.007
A7H	34.3	0.031	0.040

Table 3 Experimentally estimated increments of the threshold stresses $\Delta\sigma_{th}$, $\Delta\sigma_{th}(P)$ and $\Delta\sigma_{th}(S)$ at various temperatures (MPa).

		100 °C	150 °C	200 °C
$\Delta\sigma_{th}(P)$	A7L−A3L	10.1	8.5	6.6
	A7H−A3H	10.2	8.4	6.8
$\Delta\sigma_{th}(S)$	A3H−A3L	13.1	6.1	4.2
	A7H−A7L	13.2	6.0	4.4
$\Delta\sigma_{th}$	A7H−A3L	23.2	14.5	11.0

Table 4 Calculated Orowan stress σ_{or} and detachment stress σ_d for the alloys.

| Specimens	100 °C				200 °C			
	σ_{or}, MPa	σ_d, MPa	$\Delta\sigma_{or}$, MPa	$\Delta\sigma_d$, MPa	σ_{or}, MPa	σ_d, MPa	$\Delta\sigma_{or}$, MPa	$\Delta\sigma_d$, MPa
A3L	11.0	5.8	-	-	10.4	5.5	-	-
A3H	10.6	5.6	-	-	10.0	5.3	-	-
A7L	22.1	11.7	-	-	20.8	11.0	-	-
A7H	21.7	11.5	-	-	20.5	10.9	-	-
A7L−A3L	-	-	11.1	5.8	-	-	10.4	5.5
A7H−A3H	-	-	11.1	5.8	-	-	10.5	5.6

Figures
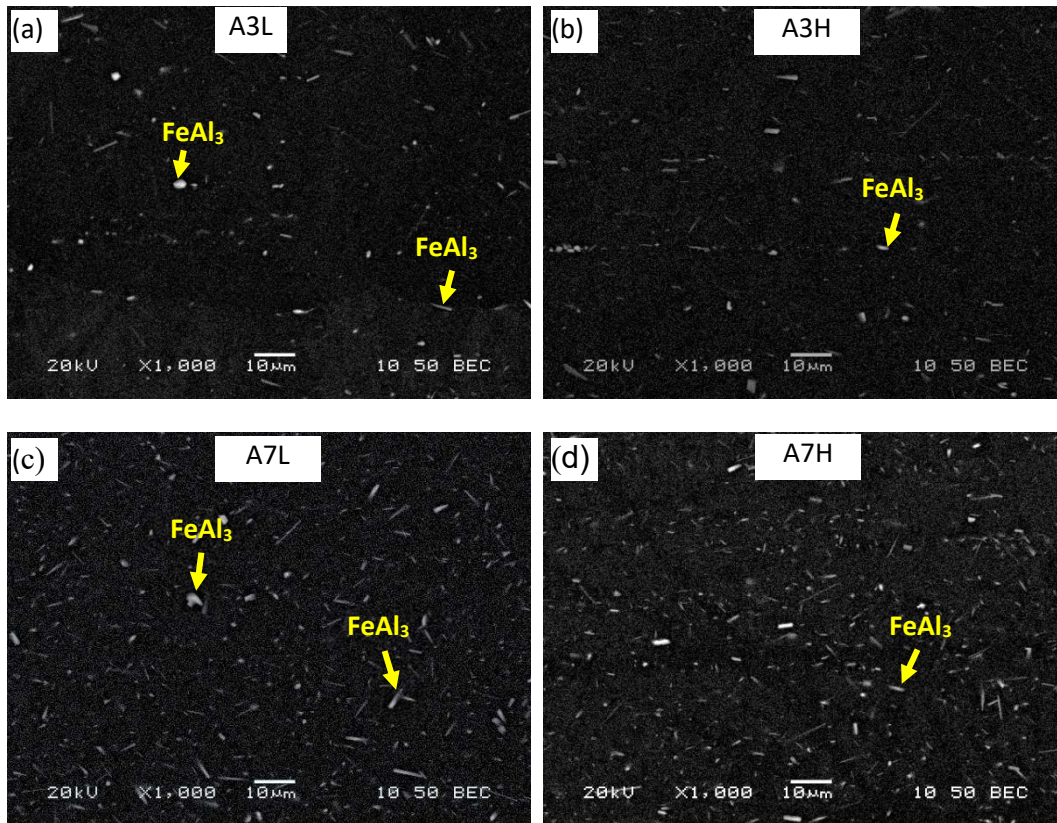
Fig. 1 SEM back-scattered micrographs of Alloy A3 (a-b) and Alloy A7 (c-d) after thermal holding treatments.
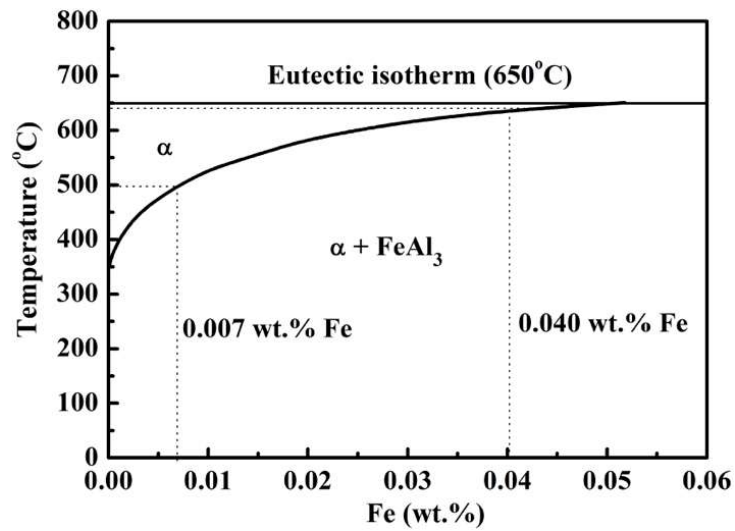

Fig. 2 Binary Al−Fe phase diagram illustrating the Fe solid solubility of at given temperature and Fe content [24].
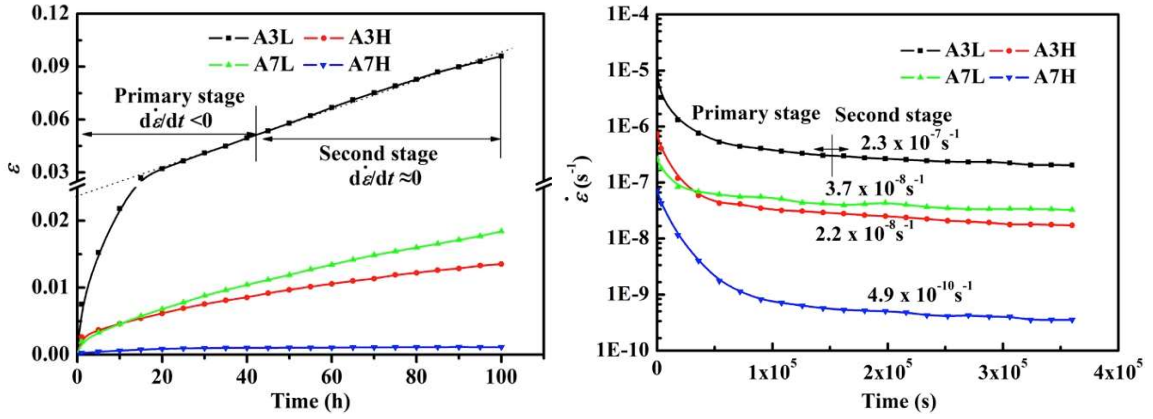
Fig. 3 Typical compressive creep curves of the alloys: (a) creep strain (ε) and (b) instantaneous creep rate ($\dot{\varepsilon}$), tested at 100 °C and an applied load of 45 MPa.
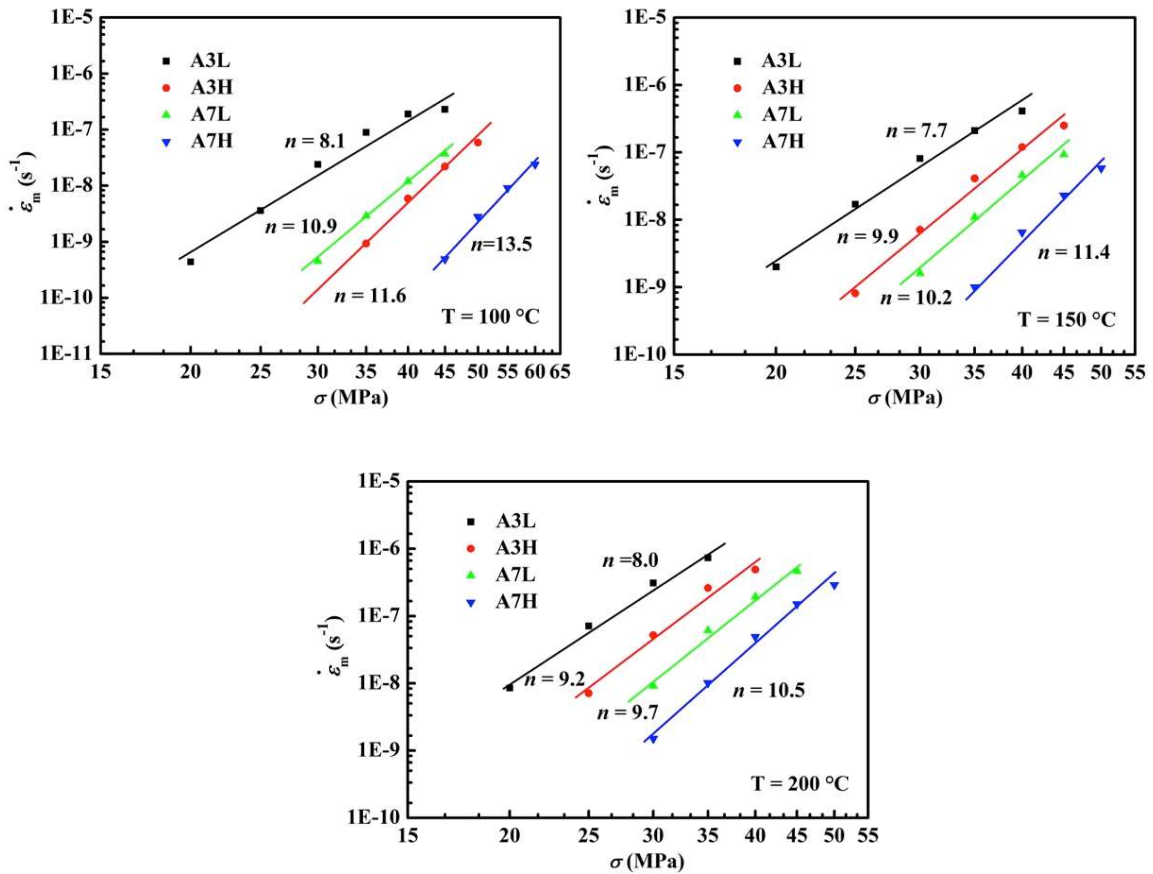

Fig. 4 Variations of the minimum creep rate $\dot{\varepsilon}_m$ with applied stress σ for alloys tested at 100 °C (a), 150 °C (b) and 200 °C (c).
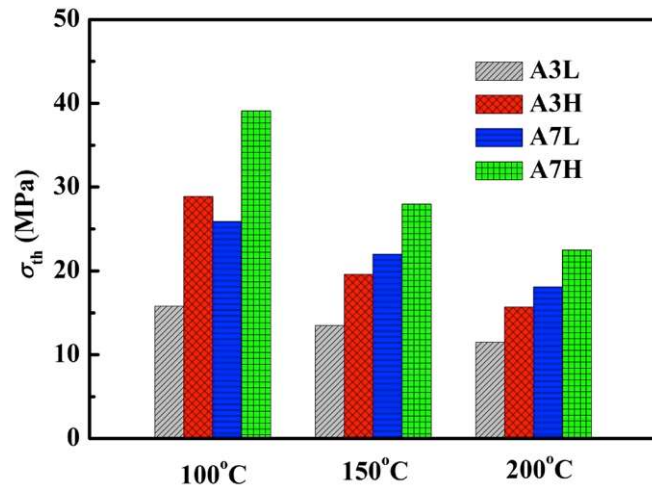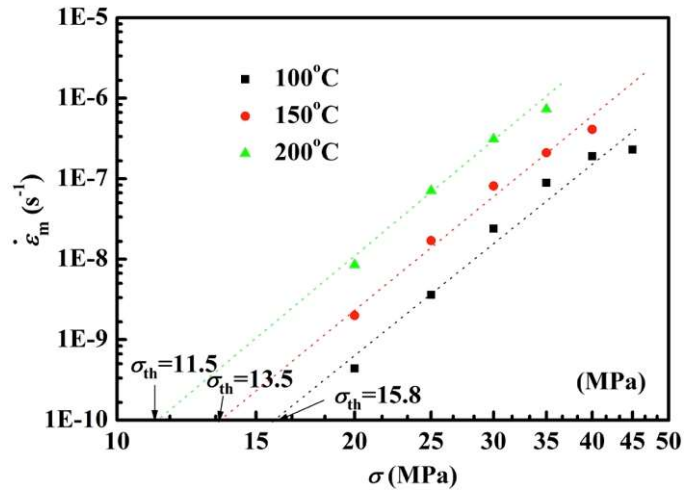
Fig. 5 Determination of the threshold stresses by the linear fitting of $\log \dot{\varepsilon}_m$ against $\log \sigma$ for A3L alloy (a) and the threshold stress σ_{th} of all of the alloys at the three test temperatures (b).
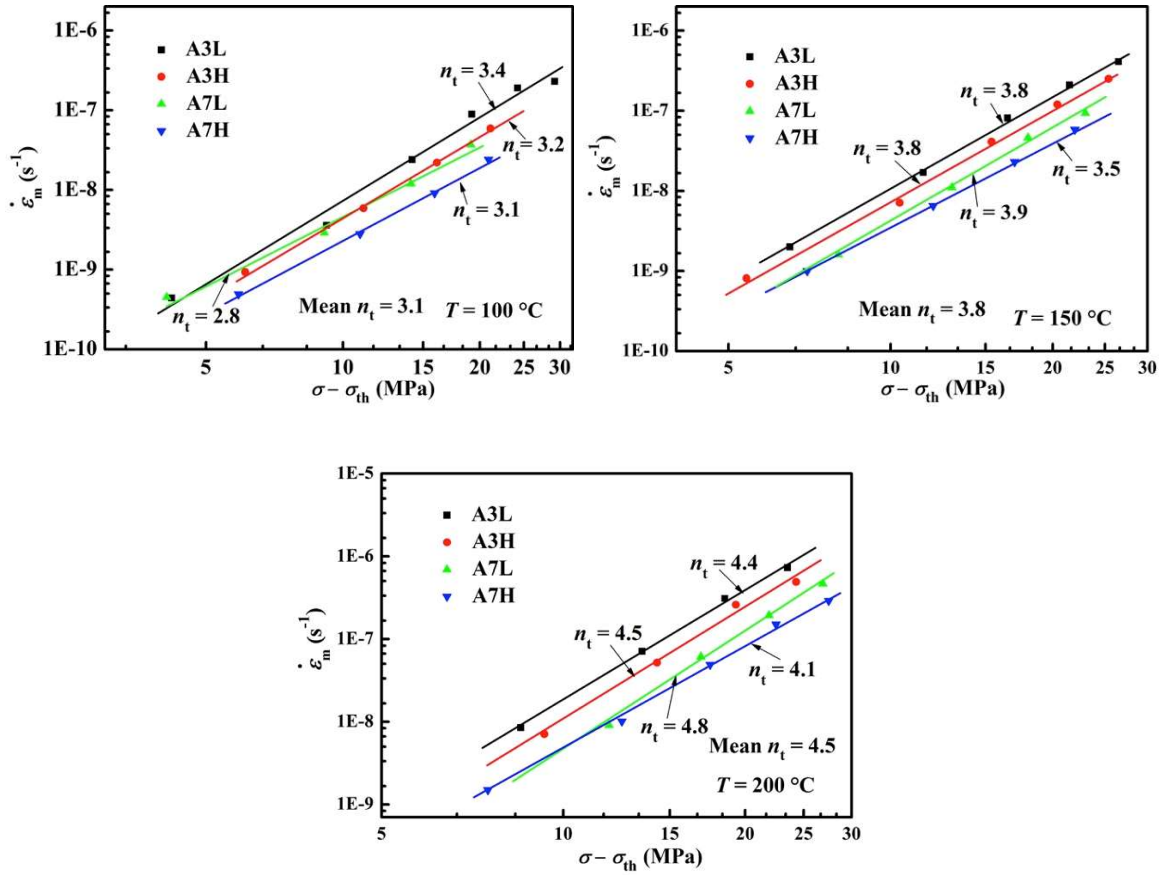
Fig. 6 Logarithmic plots of the minimum creep rate $\dot{\varepsilon}_m$ vs the effective stress σ-σ_{th} for alloys at three temperatures: 100 °C (a), 150 °C (b), and 200 °C (c).
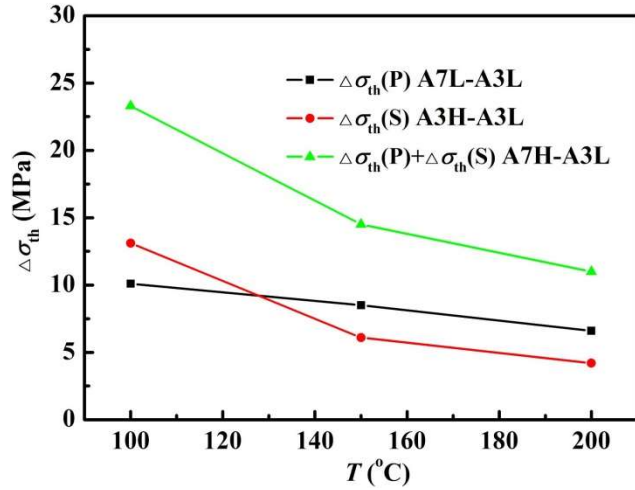
Fig. 7 Increment of the threshold stress $\Delta\sigma_{th}$ due to FeAl$_3$ particles and Fe solutes with increasing temperatures.
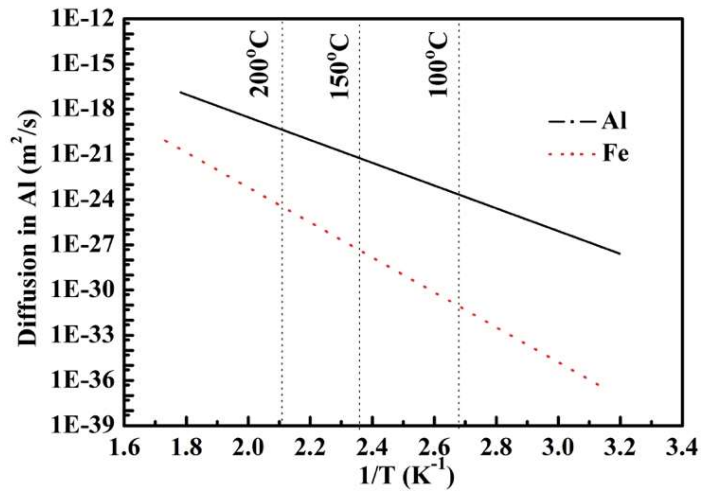

Fig. 8 Diffusion rate of Al and Fe in aluminum as a function of the reciprocal temperature [12].